



A dual-porosity model for the study of chemical effects on the swelling behaviour of MX-80 bentonite

Zhenze Li¹ · Grant Su² · Quinn Zheng² · Thanh Son Nguyen²

Received: 13 September 2018 / Accepted: 3 January 2019 / Published online: 9 February 2019
© The Author(s) 2019

Abstract

Significant chemical influence on the swelling potential of MX-80 bentonite was observed during swelling tests where specimens were hydrated with highly concentrated brine. The maximum swelling pressure for specimens hydrated with brine was about 30% of the maximum swelling pressure for the same specimens hydrated with de-ionized water. The maximum swelling pressure was attained within tens of hours of brine infiltration and further decreased by half within a year. A fully coupled hydro–mechanical–chemical (HMC) dual-porosity model is proposed in this paper to interpret the swelling behaviour of MX-80 when infiltrated with brine. The dependence of hydraulic and mechanical properties on such factors as porosity, salinity and water content was investigated. A nonlinear elastic constitutive model was proposed to correlate the swelling pressure with the variation in the microporosity. The chemical effects on the mechanical behaviour were coupled at the micropore level. A number of relationships have been developed for MX-80, i.e. micropore permeability as a function of void ratio, water retention characteristics of micropores and macropores, micropore dependence on water content and the diffusion coefficients of the two types of pore structure. The proposed model was successful in reproducing both quantitatively and qualitatively the experimental results from two sets of infiltration experiments on compacted MX-80 bentonite.

Keywords Bentonite · Brine · Coupled processes · Dual porosity · Salinity · Swelling

1 Introduction

Bentonite has been widely considered as seal materials in nuclear waste disposal facilities [1, 13, 15, 43, 44, 53]. Bentonite is primarily composed of montmorillonite minerals. Montmorillonite is characterized with high specific surface area, high swelling potential and a strong tendency to bound water. These characteristics could ensure a very low permeability and high sealing capacity of the bentonite when wetted. Deep geological disposal is being considered in Canada and many other countries for the long-term management of nuclear waste. Deep geological repositories (DGR) for nuclear waste rely on a system of engineered and natural barriers to contain and isolate the waste.

Bentonite-based buffer and seal engineered barrier systems (EBS) are major components of this multi-barrier system. Once emplaced between the waste containers and the host rock, the swelling potential of the bentonite upon saturation with porewater from the host rock is relied on in order to seal gaps and fissures that may exist in the EBS itself and/or the surrounding host rock in the vicinity of the waste emplacement areas. The chemical characteristics of the pore fluid, i.e. pH, salinity, cation types, have been shown to affect the swelling behaviour of the bentonite [13, 21, 32, 49]. In Canada, the porewater in deep geological formations is characterized by high salinity. For example, the total dissolved solids (TDS) of the porewater at the Bruce site, Ontario, where a DGR for low- and intermediate-level wastes is being proposed, are up to 450 g/L at depths of more than five hundred metres. The highly concentrated brine in the host rock would seep into the EBS, triggering complex hydraulic (H)–mechanical (M)–chemical (C) processes that could affect the swelling potential of the bentonite. These HMC processes are

✉ Thanh Son Nguyen
son.nguyen@canada.ca

¹ Geoenvironment Consulting, Ottawa, Canada

² Canadian Nuclear Safety Commission, Ottawa, Canada

coupled and are far more complex than the swelling behaviour of bentonite infiltrated with de-ionized (DI) water. Herbert et al. [18] found that brine with elevated salt concentration in contact with MX-80 bentonite can decrease its swelling pressure to a steady-state value that might take years to be reached. Swelling pressure tests were conducted at Queen's University, Canada, in collaboration with the CNSC [42]. The results showed that the swelling pressure of MX-80 bentonite hydrated with DI water reached a plateau in a monotonous manner after approximately 1 month. On the other hand, for the same specimens hydrated with brine, the swelling pressure increased to a maximum value within tens of hours but reduced slowly to an equilibrium state after approximately 1 year. The final values of the swelling pressure of specimens hydrated with brine are approximately one order of magnitude smaller compared to the DI case. In order to interpret the observed chemical effects on the swelling behaviour of bentonite, the authors have developed in this paper a fully coupled HMC model that takes into account the dual-porosity structure of the bentonite. Although most of the assumptions used in this work might be applicable to other types of bentonite, the focus is on MX-80, a sodium bentonite.

Hydraulic–mechanical (HM)- or thermal–hydraulic–mechanical (THM)-coupled models incorporating dual-porosity structures have been developed and successfully validated against experimental observations in a number of pioneering studies [3, 12, 16, 17, 19, 37, 46, 47, 50, 55]. Momentum and mass conservation equations for each pore structure are required for the simulation of water flow and vapour transport processes [37]. Dual-porosity-based hydraulic flow and chemical transport models were reported with respect to unsaturated bentonite soils [31, 33, 41, 54]. Recently, a HMC-coupled dual-porosity model was developed by Musso et al. [34] to address the volume change of expansive soil under cycling of chemical permeation. This approach, although only addressing the fully saturated situation, provides an excellent framework to interpret the chemical influences on the swelling behaviour of bentonite [8]. In the present study, the authors developed a HMC-coupled model taking into account the dual-porosity structure of bentonite. The model was based on the dual-porosity HMC-coupled model from Musso et al. [33], but it was extended to address a full spectrum of hydraulic flow in both unsaturated and saturated states. Two types of pore structures were considered: the micropores within the clay aggregates and the macropores between those aggregates. The model considers porewater flow and solute transport in both pore structures and hydraulic and chemical exchange between the two structures through a semi-permeable membrane. This paper is structured as follows: (1) characterization of hydraulic and

transport properties of bentonite; (2) derivation of governing HMC equations; (3) development of finite element (FE) models; and (4) mathematical simulation of swelling tests.

1.1 Characterization of hydraulic and transport properties of bentonite

1.1.1 Double-porosity in bentonite

The microstructure of bentonite has been the focus of many porosimetric and microscopic studies [2, 9, 30, 31, 34, 45]. An illustration of the bentonite microstructure is shown in Fig. 1. The fundamental structural units are the clay platelets or layers, separated by several layers of water molecules and assembled in stacks of 2–3 platelets at full saturation to about 300 platelets at high suctions [48]. The stacks are assembled together in aggregates. From the above microstructural organization, bentonite could conceivably be characterized by three types of pores: the nanopores (at nm scale) that exist between the clay platelets within a stack; the micropores (in the size range of 0.01–2 μm) between the clay stacks within the aggregate; and the macropores (in the size range of 2–300 μm) that exist between the clay aggregates and other macrograins such as quartz grains.

When water is added to an unsaturated bentonite sample, it infiltrates first into the macropores and then into the micropores and nanopores, resulting in an expansion of the aggregate. This process is involved with a subdivision of the stacks, as well as an increase in the thickness of the diffuse double layer (DDL) [48]. The DDL is generally in the scale of tens of nm to a few micrometres. The proportion of macropores in the size range of 2–300 μm reduces significantly, while micropores in the size range of 0.01–2 μm increase in a wetting cycle with DI water. Manca et al. [29] studied the microstructural evolution of bentonite and noticed a steady and quasi-linear increase in micropore volume with decreasing suction in the wetting path. Under confined conditions, the tendency for the aggregate to expand results in the development of a swelling pressure.

Concentrated polyvalent cations in infiltrating waters have been found to decrease the swelling potential of montmorillonite due to a reduction of interlayer expansion, thinner bound water, flocculation of fine minerals and contraction of aggregates [20]. This effect further contributes to the formation of macropores even when the soil is saturated, as evidenced by elevated hydraulic conductivity [20, 29]. Melkior et al. [30] studied the microstructure of various types of bentonite and found that a gel phase in the material governs the pore structure. A homogeneous gel structure is developed in low salinity (typically NaCl,

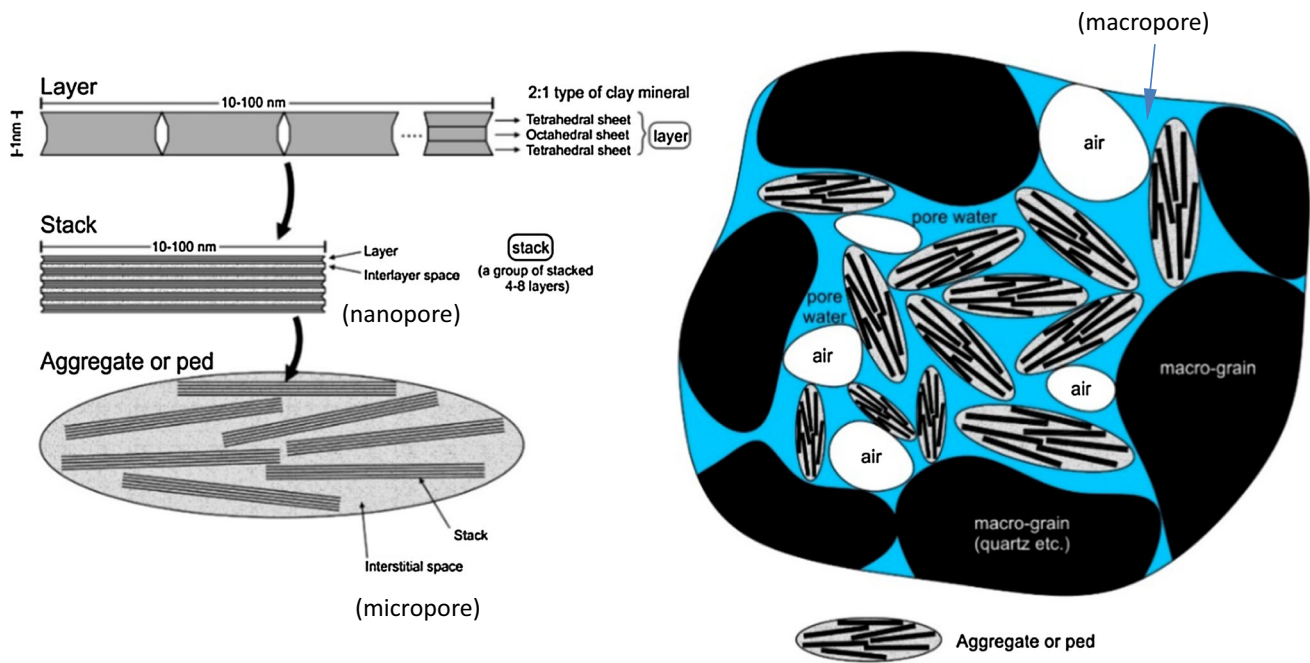


Fig. 1 Illustration of the microstructure of bentonite (from [36])

10^{-3} M), showing an isotropic network of clay stacks with 5–10 clay layers. In a concentrated solution (NaCl, 10^{-1} M), a heterogeneous structure consisting of thicker mineral stacks (40–60 clay layers) is observed. It is shown that increased salinity results in thicker stacks of mineral layers and a closer, denser pack of clay aggregates, which can be illustrated by Fig. 2b, where brine causes the macropore fraction to increase compared to DI water. The simultaneous transport of water and solute in the double structures takes place in such a manner that water moves faster than solute in the micropore and causes the aggregate to expand in the early stage; the solute gradually migrates into the micropore at a later stage and causes the aggregate to shrink to an equilibrium state. This is illustrated in Fig. 2c. The chemical influence on the dynamics of the double structures appears to be somewhat reversible, as leaching of salts from porous media can cause enhanced dispersion and deflocculation in clay slurry [24], which turns out to enhance its swelling potential [32, 34].

The mathematical model that is described in this paper is based on the multiple porosity concept as previously discussed. We did not take into account the nanopore and only consider the micropore structure within an aggregate and the macropore structure between the aggregates. This simplification seems to be sufficient in order to explain the main phenomena associated with the swelling of compacted bentonite [17]. Microstructural morphological studies on bentonite under wetting paths indicate a gradual reduction of the macropores and steady cumulative growth in the abundance of micropores [29]. As shown in Fig. 2c,

when full saturation occurs with DI water, the macropores would practically disappear. However, when the bentonite is saturated with brine, the reduction of macropores is much less pronounced with increasing salinity in the pore fluid, as demonstrated in Fig. 2a, b.

1.2 Hydraulic conductivity of a dual-porosity medium infiltrated with brine

Assuming that Darcy's law is applicable, porewater flow in a dual-porosity medium depends on the hydraulic conductivity of the bulk medium, which is a function of the hydraulic conductivity associated with each pore type. In a dual-porosity medium, the effective saturated hydraulic conductivity (k_{eff}) representative of the overall medium could be expressed as the arithmetic mean of the respective components associated with each porosity type, assuming that flow takes place in parallel in each porosity type:

$$k_{\text{eff}} = \frac{e_m}{e_m + e_M} k_s^m + \frac{e_M}{e_m + e_M} k_s^M \quad (1)$$

where e is the void ratio, k_s is the saturated hydraulic conductivity and the subscripts m and M , respectively, indicate the micropore and the macropore.

We will now propose a methodology to estimate the three types of hydraulic conductivity considering the influence of salinity of the infiltrating water. We start first with the adoption of the semi-theoretical equation from Kozeny [22] and Carman [6] for a single-porosity medium:

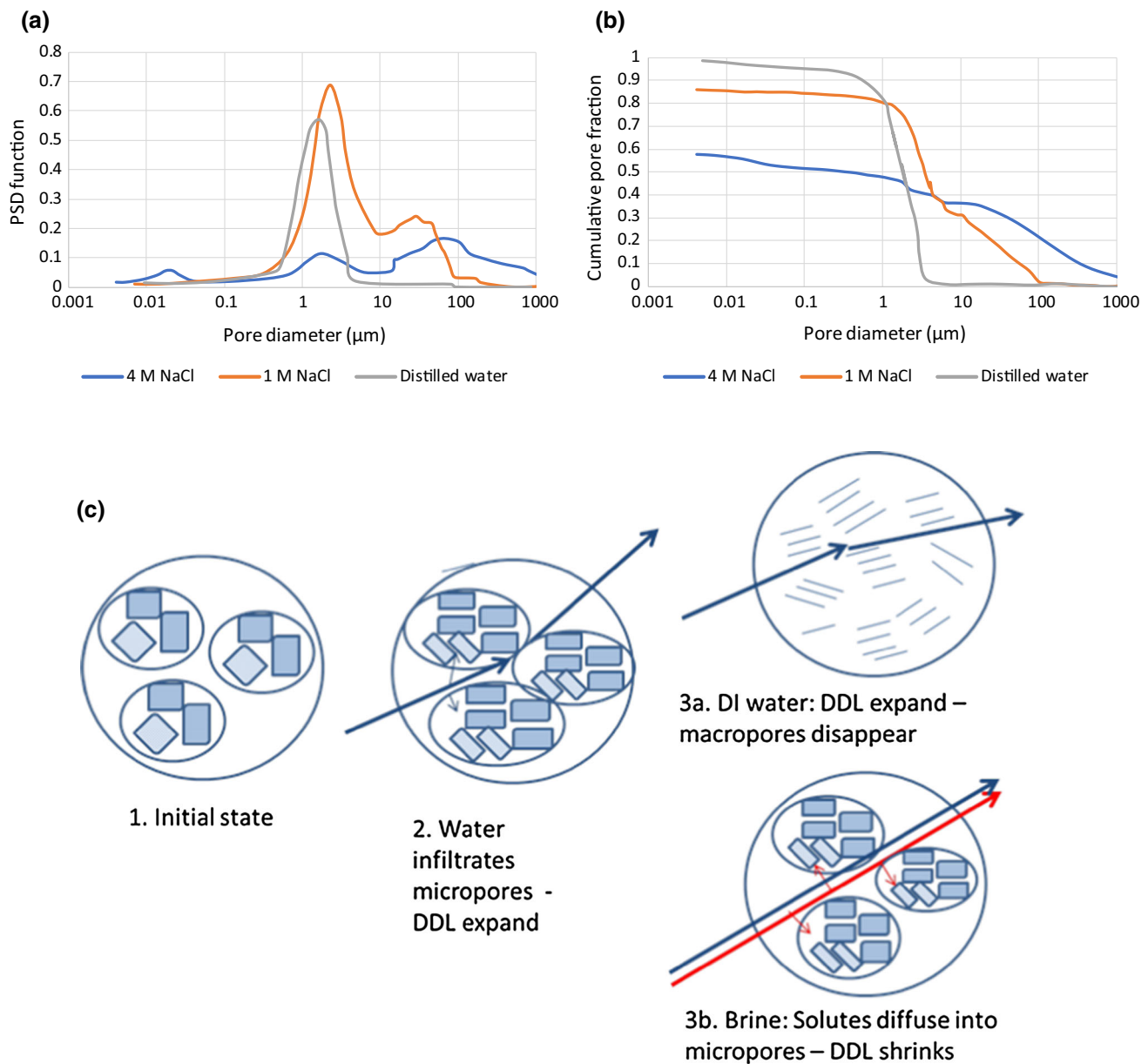


Fig. 2 **a** Pore size distribution, **b** cumulative pore fraction of sand/bentonite mixture saturated with various concentrations of pore fluids (after Manca et al. [29], initial void ratio $e = 0.78$) and **c** schematic diagram for sequential development of structures and water (blue line) and solute (red line) migrations under brine infiltration (color figure online)

$$k = \frac{\gamma}{\mu C_{kc} S^2} \frac{e^3}{1 + e} \quad (2)$$

where k is the saturated hydraulic conductivity (m/s) of the single-porosity medium, γ is specific gravity, μ is pore fluid viscosity (Pa s), S is specific surface area in unit volume of solid phase, C_{kc} is the Kozeny–Carman empirical coefficient, e is void ratio. Using experimental data from various sources for bentonite infiltrated with DI water (Fig. 3), the effective hydraulic conductivity (m/s) of the bulk medium can be represented by a power law function that is very similar to the Kozeny–Carman equation:

$$k = 10^{-13} \frac{e^{3.74}}{1 + e} \quad (3)$$

We have $\frac{\gamma}{\mu} = 7.6 \times 10^6$ 1/m s. The specific surface area S in unit volume of typical MX-80 can be calculated from specific surface area (SSA) value of $561 \text{ m}^2/\text{g}$ [5], which leads to $S = \text{SSA} * \gamma_s \times 10^6 = 1.51 \times 10^9$ 1/m.

Therefore, the model constant C_{kc} can be estimated for bentonite as

$$C_{kc} = \frac{\gamma}{\mu S^2} 10^{13} e^{-0.74} = 33.3 * e^{-0.74} \quad (4)$$

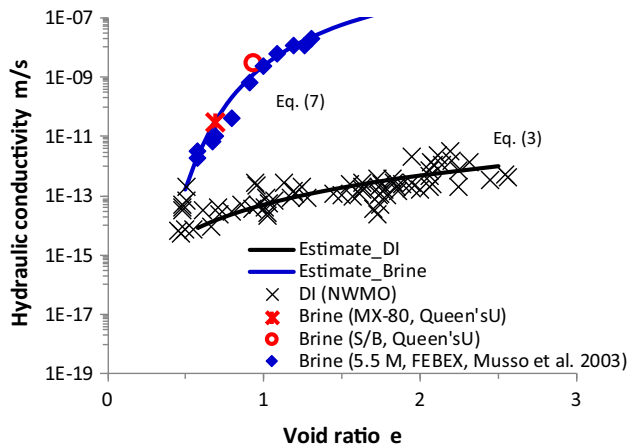


Fig. 3 Dependence of hydraulic conductivity of bentonite on void ratio and salinity (solid symbols with chemical concentrations represent the FEBEX bentonite from Musso et al. [32]; the MX-80 data from Queen's University [42]; the DI_NWMO data from Man, Martino [28])

This C_{kc} value could be much larger than the well-recognized value of 5 for packed sandy soils as indicated by Carrier III [7]. This is likely due to the thick electric double layer of clay particles, that greatly hinders the transmissivity of compacted clay, through electric–hydraulic-coupled effects [25] and thus increases the C_{kc} factor. It is shown by the above analysis that the Kozeny–Carman equation is suitable for permeability estimation regarding the specific case of MX-80 bentonite hydrated with DI water.

As previously discussed, when bentonite is saturated with DI water, the macropores practically disappear; therefore, $k_{eff} = k_s^m$, and the effective hydraulic conductivity of bentonite in this case, and as represented by Eq. 3, is assumed to be equal to the micropore permeability. Therefore, the saturated micropore hydraulic conductivity k_s^m is assumed to be given by:

$$k_s^m = 10^{-13} \frac{e_m^{3.74}}{(1 + e_m)} \quad (5)$$

e_m , the micropore void ratio could be determined by the micropore gravimetric water content (w^m) as

$$e_m = w^m G_s \quad (6)$$

Note that w^m is distinct from the total water content w and is governed by the osmotic suction of chemical solution.

The effective hydraulic conductivity of compacted MX-80 bentonite with brine was determined by experiments. The data that come from different sources as shown in Fig. 3 can best fit with an empirical equation of

$$k_{eff} = 10^{-9} e^{11.86} \quad (7)$$

where e is the total void ratio given as $e = e_m + e_M$.

Being orders of magnitude higher than the micropore permeability, the macropore hydraulic conductivity with brine infiltration could be treated as equivalent to the overall effective permeability of the sample, i.e.

$$k_s^M \approx k_{eff} \quad (8)$$

1.3 Chemical transport properties: tortuosity and diffusion

For the macropores, the free diffusion coefficient is assumed to prevail, i.e. $D_e = D_0$. For the micropores, tortuosity significantly affects the diffusion of solutes. The relation between tortuosity and diffusion in the micropores can be illustrated by looking at the 1-D solute transport equation:

$$\frac{\partial C}{\partial t} = \frac{D_e}{n + \rho_b K_d} \frac{\partial^2 C}{\partial x^2} = D_a \frac{\partial^2 C}{\partial x^2} \quad (9)$$

where n is porosity, ρ_b is bulk density, K_d is the partition coefficient that takes into account sorption of the solutes on the solid phase, C is solute concentration, D_e is the effective diffusion coefficient, D_a is the apparent diffusion coefficient ($D_a = \frac{D_e}{n + \rho_b K_d}$), t is time and x is the length.

For non-sorptive chemicals like Cl^- , ClO_4^- and I^- , K_d is negligible. Then we can simplify the diffusion coefficient into

$$D_e = D_a n \quad (10)$$

Many test data [4, 35, 51] show an exponential decay or power law relationship (Fig. 4) between the ratio of apparent diffusion coefficient to free diffusion coefficient (D_0) and porosity for bentonite infiltrated with DI water or slightly salt solution in the following form:

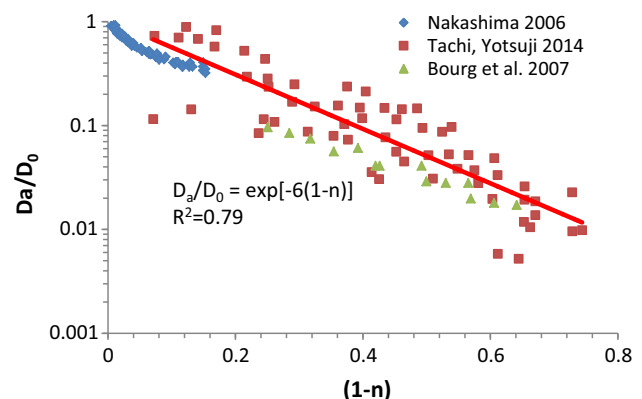


Fig. 4 Diffusion coefficients of non-sorptive species in compacted bentonite

$$\frac{D_a}{D_0} = \exp[-6(1-n)] \quad (11)$$

Therefore,

$$D_e = nD_0 \exp[-6(1-n)] \quad (12)$$

1.4 WRC for MX-80 bentonite

Soil suction is defined as the energy required for extracting a unit volume of water from a soil in order to overcome retention mechanisms that exist in that soil [14]. For the current problem under study, three distinct water retention mechanisms are considered: water adsorption, capillary retention and osmosis. The total suction (S_u) is equal to the sum of matric suction (p_m) and osmotic suction (π), according to the definition of soil suction by the International Society of Soil Science and others [23, 52]. Water adsorption upon clay minerals at high suction levels and capillary retention at lower suction levels [10, 48] are responsible for matric suction. Water adsorption is mainly governed by the physicochemistry of clay minerals and takes place in the intra-aggregate micropores in terms of electric double layers between the clay stacks [48]. Experiments have shown that the total void ratio or dry density has no effect on the WRC of MX-80 bentonite at suction levels higher than 10 MPa, suggesting that the predominant mechanism of water retention is adsorption in that high suction range. The second mechanism of retention is mainly attributable to capillarity effects in the inter-aggregate macropores when the soil approaches a saturated state, e.g. suction becomes less than the air entry value (AEV). For the purpose of modelling water flow in MX-80 within a dual-porosity framework, we need relationships for the WRC in both types of pores that take into consideration the above three types of water retention mechanisms. These relationships are derived as follows.

1.4.1 Macropore WRC

The macropore WRC is derived from Dieudonne et al. [10], who proposed a model for the macropore water retention curve and calibrated it successfully against experimental results for MX-80 bentonite. Their approach is based on the following assumptions:

- (1) Adsorption and capillarity are the respective mechanisms for water retention in the micropore and macropore; osmosis is not considered;
- (2) the AEV α could be expressed as a function of macropore void ratio e_M , $\alpha = 0.2/e_M$ (MPa);
- (3) the micropore void ratio (e_m) could be expressed as a function of water ratio (ratio of volume of water over

- solid volume) e_w , $e_m = 0.48(e_w)^2 + 0.1e_w + 0.31$;
- (4) the water ratio is dependent on the gravimetric water content, $e_w = G_s w$.

Based on the above assumptions, Dieudonné et al. [10] fitted the van Genuchten equation to experimental data. The data points from those authors for compacted MX-80 bentonite at a dry density of 1.6 g/cm³ are plotted as square dots in Fig. 5. We applied the following Brooks–Corey equation in order to best fit the data points as shown in Fig. 5:

$$S_e = (0.4S_u)^{-\frac{1}{1.6}} \quad (13)$$

where S_e is the saturation degree.

1.4.2 Micropore WRC

The total suction of MX-80 bentonite hydrated with both DI water and brine solution has been measured by the chilled mirror technique [42] and are plotted against gravimetric water content as shown in Fig. 6. The chilled mirror technique measures the vapour pressure and gives the total suction of the bentonite specimen. For the case of DI water, no osmotic suction exists; therefore, the total suction is equal to the matric suction. For the case of brine, assuming thermodynamic equilibrium, the measured total suction S_u should be the same for both pore structures. Furthermore, due to the relatively short duration of the WRC test, the amount of solutes migrating into the micropore could be neglected. Therefore, osmotic suction in the micropore could be neglected, and matric suction in the micropore would be approximately equal to the total suction (i.e. $p_m = S_u$). We propose the following empirical relationship for the WRC of MX-80 bentonite hydrated with DI water:

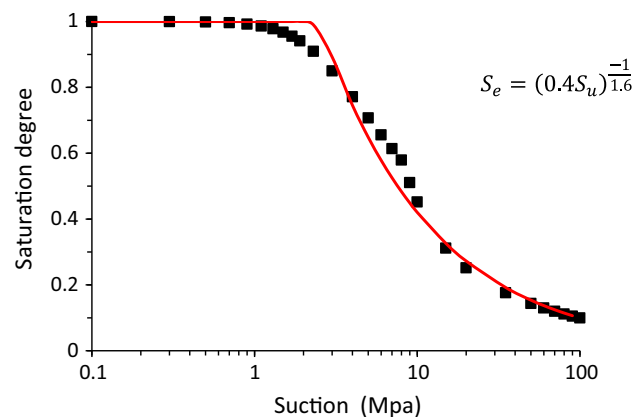


Fig. 5 The predicted WRC (line) for the macropore by the Brooks–Corey model $S_e = (\alpha S_u)^{-n}$ with $\alpha = 0.4 \text{ MPa}^{-1}$, $n = 0.625$ and $\rho_d = 1.6$ fitted to experimental data on MX-80 (square dots) from Dieudonne et al. [10]

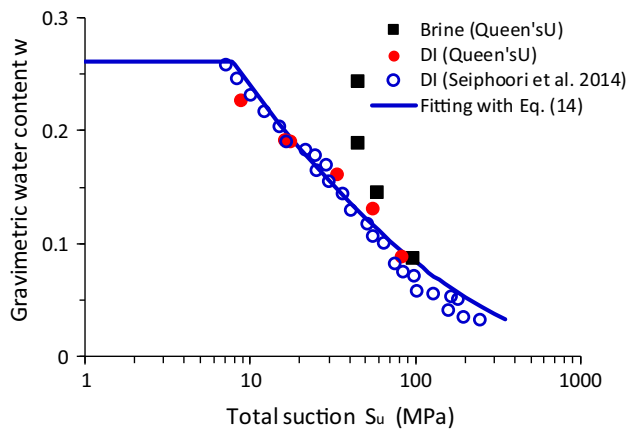


Fig. 6 WRC of MX-80 bentonite with respect to total suction

$$\sqrt{w} = -0.2 * \log\left(\frac{p_m}{S_{ut}}\right), \quad S_{ut} = 2800 \text{ for DI water} \quad (14)$$

where p_m is matric suction, w is water content and S_{ut} is the suction at which $w = 0$. As previously discussed, when MX-80 is infiltrated with DI water, the clay aggregates break down and eventually all macropores disappear. Therefore, Eq. (14) is regarded as representative of micropore WRC for DI water.

$$S_e = (0.4S_u)^{\frac{-1}{1.6}}$$

The WRC for the case of brine as shown in Fig. 6 is not in its equilibrium state when bentonite is in contact with brine solution, since those measurements were performed in a relatively short period of time. With the migration of chemicals into the micropore space, the WRC will evolve due to the gradual increase in osmotic suction in the micropores. In this study, we address this chemical-dependent variation of micropore WRC by generalizing Eq. (14). This generalization is done by making the suction toe (S_{ut}) dependent on the solute concentration inside the micropore. An exponential function is proposed for this relationship as below, and its parameters were obtained by calibration against swelling test data from Queen's University by an iterative regression method:

$$S_{ut} = S_{ur} + \vartheta e^{-A * C^m} \quad (15)$$

where the calibrated model parameters $S_{ur} = 100$ MPa; $\vartheta = 2700$ MPa; $A = 0.0006$; C^m is the micropore solute concentration in the unit of mol/m^3 .

1.5 Swelling pressure at various dry densities and salinities

Figure 7 shows the variation of swelling pressure of MX-80 bentonite with effective montmorillonite dry density (EMDD) at various salinity conditions. EMDD is defined

as the mass of swelling clay minerals present in a sample divided by the volumes of voids and swelling clay minerals. Brine generally leads to a decrease in swelling pressure for bentonite. The logarithm of swelling pressure is found to change linearly with EMDD. The test data for model water obtained from Queen's University follow the general trend as reported in existing studies [11]. As discussed later, in the case of brine infiltration, the data from Queen's University show that the swelling pressure increases rapidly to peak values. Those peak values are shown in Fig. 7a. At very long periods of time (of the order of 1 year or more), the swelling pressure decreases to smaller steady-state values, as shown in Fig. 7b. That long-term reduction in swelling pressure is likely attributed to the chemistry of the model water, i.e. the high concentration of Ca, Mg, K. Herbert et al. [18] observed a similar trend in swelling pressure decrease under chemical influence.

1.6 HMC-coupled model for MX-80 bentonite

1.6.1 Key assumptions

(a) Dual-porosity structure

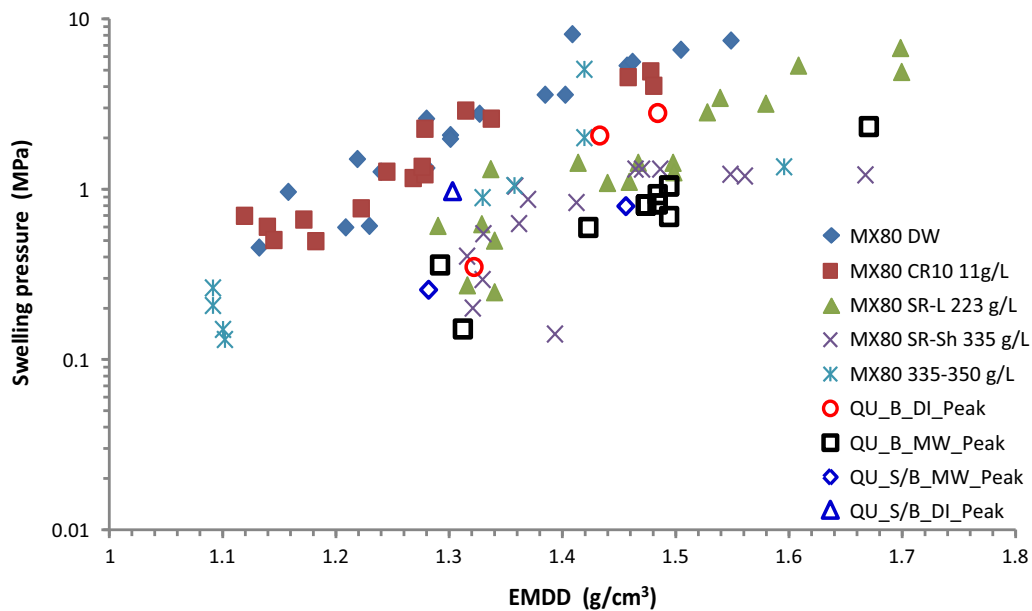
As discussed previously, two types of pore structures, the intra-aggregate micropores and the inter-aggregate macropores, are considered in this study. The relevant proportion of each porosity varies with both matric suction and osmotic suction. The microstructural volume change could cause changes in various parameters such as hydraulic conductivity, water retention capacity, diffusion coefficient and swelling pressure measurement. Therefore, a conceptual model was established in the dual-porosity framework as shown in Fig. 8. According to this conceptual model, fluid flow and chemical transport processes occur simultaneously in both pore structures, with exchange of fluid and chemicals between the two structures.

(b) Chemical-dependent WRC

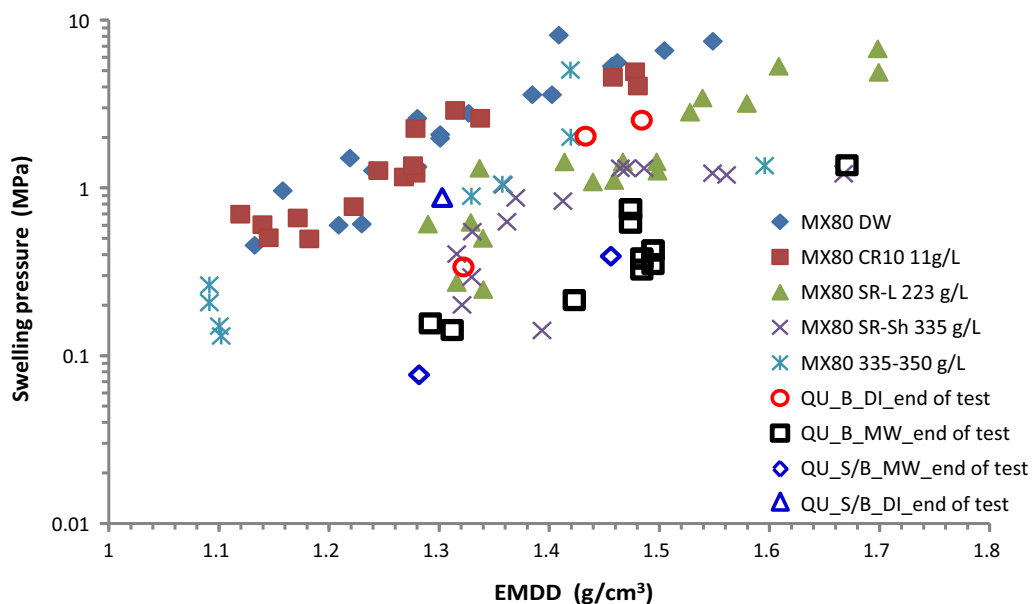
Hydration with brine solution through the macropore may cause perturbation to the salinity in the micropore. The salts entering the micropore modify the electrochemical equilibrium in the electric double layer in the micropore space, resulting in a change in the WRC. Therefore, an appropriate treatment of the chemistry-dependent WRC is critical to reflect the time-dependent dynamic process of clay–chemical interactions.

(c) Water content-dependent microporosity

In highly expansive bentonite, water is preferentially sorbed to the mineral surface and interlayers due to electrochemical interactions. Navarro et al. [38] believed that at



(a) Peak values of swelling pressure from Queen's University



(b) Steady-State values of swelling pressure from Queen's University

Fig. 7 Variation of swelling pressure of MX-80 bentonite with effective montmorillonite dry density (EMDD) for various salinity conditions—Modified from [11]; QU stands for Queen's University, with peak values reported in **a** and steady-state values reported in **b**

high suction levels, most of the water is sorbed water in the micropores, and the water in the macropores can be drained completely even though the micropores remain saturated. In this study, the microporosity is assumed to be solely dependent on the gravimetric water content when matric suction $S_u > AEV$. The swelling of bentonite is primarily attributed to the penetration of water into the diffuse layer and interlayer space of clay minerals (or intra-aggregate

space). Therefore, the microporosity varies with the change in water content in the micropore. This assumption is consistent with Navarro et al. [39].

(d) Membrane effect

Semi-permeable membrane effect is prominent for bentonite in contact with saline water [21, 25, 27]. The membrane has a filtering effect: it delays movement of

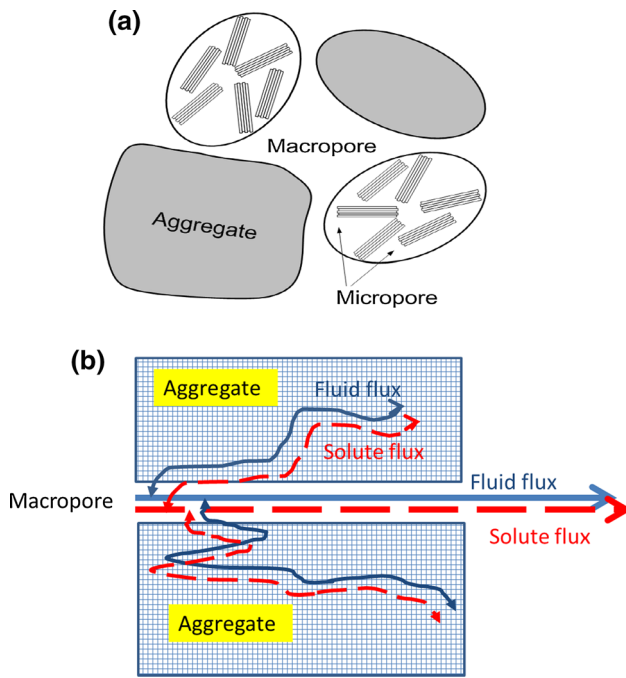


Fig. 8 Schematic illustration of **a** the dual-porosity structure in pore space and **b** the conceptual model for fluid and solute fluxes and exchange between pore structures

solutes with respect to the flow of water into the micropores.

1.7 Hydraulic flow equations

Let us consider a representative element of porous media with a single-porosity structure, and let n be porosity, S_e the degree of saturation, ρ_l the fluid density, G_s the specific gravity of solid and w the gravimetric water content. By assuming that G_s stays constant over time (i.e. no dissolution or precipitation reactions taking place), we can write the following equation of fluid mass conservation:

$$\frac{\partial}{\partial t}(\rho_l n S_e) - \nabla \cdot \frac{k_s k_r}{\mu} \rho_l \nabla P = Q \quad (16)$$

where P is the net pore pressure, k_s is saturated intrinsic permeability, k_r is the relative permeability and Q is the source term. The net pore pressure P is composed of water pressure (p) and osmotic suction (π) in the form of

$$P = p - \pi \quad (17)$$

where $p = u_a - p_m$ if $S_e < 1$.

In the saturated state, p represents the pore pressure measurable by pore pressure transducer. The relationship between different suction and pore pressure parameters is as follows. Let S_u be the total suction, then $S_u = p_m + \pi$. The matric suction $p_m = u_a - p$, with u_a the air pressure, considered as atmospheric (0), and p the water pressure,

then $p = -p_m$. Then, the net pore pressure P is the negative of total suction as $P = -S_u = p - \pi$

From fundamental phase relationship, we get

$$n S_e = (1 - n) G_s w \quad (18)$$

Differentiation of the first term of Eq. (16) leads to

$$\begin{aligned} \frac{\partial}{\partial t}(\rho_l n S_e) &= \frac{\partial}{\partial t}[\rho_l (1 - n) G_s w] = (1 - n) G_s \frac{\partial}{\partial t}(\rho_l w) \\ &\quad + \rho_l G_s w \frac{\partial}{\partial t}(1 - n) \\ &= (\alpha) + (\beta) \end{aligned} \quad (19)$$

Since pore fluid is compressible and water content is suction dependent, we can further differentiate the above equation with respect to net pore pressure P as

$$(\alpha) = (1 - n) G_s \frac{\partial}{\partial P}(\rho_l w) \frac{\partial P}{\partial t} \quad (20)$$

The osmotic suction is dependent on solute concentration C in the form of

$$\pi = k_c C \quad (21)$$

where $k_c = RT$ for dilute salt solutions ($C < 0.1$ M), R is ideal gas constant (8.314 kPa L/(K mol)), T is temperature (K), in which case $k_c = 8.314 \text{ kPa} \cdot \text{L}/(\text{K mol}) \cdot 300 \text{ K} \approx 2.5 \text{ MPa} \cdot \text{L}/\text{mol}$. For concentrated brine, this formula has to be corrected, i.e. 1 M NaCl solution has an osmotic suction of 4.8 MPa. For multivalent chemical mixtures such as the model saline water used in this study ($C = 4.6 \text{ mol/L}$ in terms of total molarity of chemicals including 2.6 M NaCl, 0.54 M CaCl_2 , 1 M KCl, 0.43 M MgCl_2 and 0.01 M MgSO_4), its osmotic suction cannot be predicted by the above correlations. Instead, it was measured to be 40.6 MPa with the chilled mirror device, suggesting a constant $k_c = 8.83 \text{ MPa} \cdot \text{L}/\text{mol}$. Note that the parameter k_c is assumed as constant in the following derivations for simplicity, though it is somewhat nonlinear within a large range of concentrations.

Then equation part (α) becomes

$$\begin{aligned} (\alpha) &= (1 - n) G_s \left[\frac{\partial}{\partial p}(\rho_l w) \frac{\partial p}{\partial t} + \frac{\partial}{\partial \pi}(\rho_l w) \frac{\partial \pi}{\partial t} \right] \\ &= (1 - n) G_s \left[\left(\chi_f \rho_l w + \frac{B}{p} \rho_l \right) \frac{\partial p}{\partial t} + \frac{\partial}{\partial C}(\rho_l w) \frac{\partial C}{\partial t} \right] \end{aligned} \quad (22)$$

where B is the slope of $w\text{-log}(S_u)$ relationship for bentonite and χ_f is the compressibility of pore fluid.

Note that fluid density varies with chemical concentration, which leads to

$$\frac{\partial}{\partial C}(\rho_l w) = w \frac{\partial \rho_l}{\partial C} + \rho_l \frac{\partial w}{\partial C} = k_2 w + k_1 \rho_l \quad (23)$$

where k_1 and k_2 are material properties that are given as $k_2 = \frac{\partial \rho_l}{\partial C}$, and $k_1 = \frac{\partial w}{\partial C} = 0$ as water content is independent of salinity.

Therefore,

$$(\alpha) = (1 - n)G_s \left[\left(\chi_f \rho_l w + \frac{B}{p} \rho_l \right) \frac{\partial p}{\partial t} + k_2 w \frac{\partial C}{\partial t} \right]. \quad (24)$$

Meanwhile,

$$\begin{aligned} (\beta) &= \rho_l G_s w \frac{\partial}{\partial t} (1 - n) = -\rho_l G_s w \frac{\partial n}{\partial t} \\ &= -\rho_l G_s w \left(\frac{\partial n}{\partial \sigma'} \frac{\partial \sigma'}{\partial t} + \frac{\partial n}{\partial P} \frac{\partial P}{\partial t} \right). \end{aligned} \quad (25)$$

Then,

$$\begin{aligned} (\beta) &= -\rho_l G_s w \left[-\frac{\partial \varepsilon_v}{\partial t} + \chi_s n \left(\frac{\partial p}{\partial t} - \frac{\partial \pi}{\partial t} \right) \right] \\ &= -\rho_l G_s w \left[-\frac{\partial \varepsilon_v}{\partial t} - \chi_s n k_c \frac{\partial C}{\partial t} + \chi_s n \frac{\partial p}{\partial t} \right] \end{aligned} \quad (26)$$

where χ_s is the compressibility of the solid matrix, ε_v is the volumetric strain and σ' is the effective stress.

Finally, we get a general expression for the flow equation in a deformable unsaturated porous medium, taking into consideration variable water density

$$\begin{aligned} G_s \rho_l w \left[(1 - n) \left(\chi_f + \frac{B}{pw} \right) - n \chi_s \right] \frac{\partial p}{\partial t} - \nabla \frac{k_s k_r}{\mu} \rho_l \nabla p \\ + G_s \rho_l w \left[n \chi_s k_c + (1 - n) \frac{k_2}{\rho_l} \right] \frac{\partial C}{\partial t} \\ + \nabla \frac{k_s k_r}{\mu} \rho_l k_c \nabla C = -G_s \rho_l w \frac{\partial \varepsilon_v}{\partial t} + Q. \end{aligned} \quad (27)$$

1.7.1 Dual-porosity flow equations

Based on Eq. (27) for a single-porosity medium, we can derive the flow equations for a dual-porosity medium as follows, where the superscripts m and M for a parameter, respectively, qualify that parameter as associated with the micropore or the macropore.

In micropore,

$$\begin{aligned} G_s \rho_l w^m \left[(1 - n^m) \left(\chi_f + \frac{B}{p^m w^m} \right) - n^m \chi_s \right] \frac{\partial p^m}{\partial t} \\ - \nabla \frac{k_s^m k_r}{\mu} \rho_l \nabla p^m + G_s \rho_l w^m \left[n^m \chi_s k_c + (1 - n^m) \frac{k_2}{\rho_l} \right] \frac{\partial C^m}{\partial t} \\ + \nabla \frac{k_s^m k_r}{\mu} \rho_l k_c \nabla C^m = -G_s \rho_l w^m \frac{\partial \varepsilon_v^m}{\partial t} + Q^m. \end{aligned} \quad (28)$$

Taking into account the constitutive relationship for the microporosity, it is inferred that the micropores are mostly saturated or are close to full saturation

($S_e^m = w^m G_s / e^m = w^m G_s / w^m G_s = 1$). Then, the flow equation for the micropores can be reduced to the Darcy's flow form

$$\frac{\partial}{\partial t} (\rho_l n^m) - \nabla \frac{k_s^m}{\mu} \rho_l (\nabla p^m - k_c \nabla C^m) = Q^m. \quad (29)$$

In macropore,

$$\begin{aligned} G_s \rho_l w^M \left[(1 - n^M) \left(\chi_f + \frac{B}{p^M w^M} \right) - n^M \chi_s \right] \frac{\partial p^M}{\partial t} \\ - \nabla \frac{k_s^M k_r}{\mu} \rho_l \nabla p^M + G_s \rho_l w^M \left[n^M \chi_s k_c + (1 - n^M) \frac{k_2}{\rho_l} \right] \frac{\partial C^M}{\partial t} \\ + \nabla \frac{k_s^M k_r}{\mu} \rho_l k_c \nabla C^M = -G_s \rho_l w^M \frac{\partial \varepsilon_v^M}{\partial t} + Q^M. \end{aligned} \quad (30)$$

The volumetric strain can be linked to the porosity variation in the following form:

$$\frac{\partial \varepsilon_v^m}{\partial t} = -\frac{\partial n^m}{\partial t} \quad (31)$$

$$\frac{\partial \varepsilon_v^M}{\partial t} = -\frac{\partial n^M}{\partial t}. \quad (32)$$

The water exchange rates between micropores and macropores take the following form:

$$Q^M = -a^M \quad (33)$$

$$Q^m = a^M \quad (34)$$

where

$$a^M = \bar{\alpha} (p^m - p^M - \pi^m + \pi^M) \quad (35)$$

where $\bar{\alpha}$ is the fluid exchange rate that is assumed to be a function of the hydraulic conductivity of the micropore, i.e. $\bar{\alpha} = N k \rho_l$, where N is a factor.

1.8 Solute transport equations

For solute transport in unsaturated porous media,

$$\frac{\partial (\theta C)}{\partial t} = \nabla (D_e \nabla C) - \nabla (v C) + Q_c \quad (36)$$

where θ is the volumetric water content, D_e is effective diffusion coefficient, v is the Darcy's velocity of the pore fluid and Q_c is the source flux of chemicals.

Since,

$$\theta = n S_e. \quad (37)$$

Then, we have

$$\frac{\partial \theta C}{\partial t} = C n \frac{\partial S_e}{\partial t} + C S_e \frac{\partial n}{\partial t} + S_e n \frac{\partial C}{\partial t}. \quad (38)$$

By neglecting the compressibility of solid matrix and pore fluid, the variation of porosity is assumed to be

dependent only on volumetric deformation due to variation of pore volume.

Therefore, we have

$$S_e n \frac{\partial C}{\partial t} = \nabla(D_e \nabla C) - \nabla(vC) + Q_c - C \left(n \frac{\partial S_e}{\partial t} + S_e \frac{\partial \varepsilon_v}{\partial t} \right). \quad (39)$$

By taking into account the chemo-osmosis effect, or the so-called semi-permeable membrane effect of expansive soils [25], the solute transport equation can be given as

$$S_e n \frac{\partial C}{\partial t} = \nabla(D_e \nabla C) - (1 - \omega) \nabla(vC) + Q_c - C \left(n \frac{\partial S_e}{\partial t} + S_e \frac{\partial \varepsilon_v}{\partial t} \right) \quad (40)$$

where ω is membrane coefficient, ρ_b is the bulk density.

In the macropore, a simplified version is obtained as follows by neglecting the semi-permeable membrane effect,

$$n^m S_e^m \frac{\partial C^m}{\partial t} = D_e \nabla^2 C^m - \nabla(v^m C^m) + Q_c^m - C^m n^m \frac{\partial S_e^m}{\partial t} - C^m \frac{\partial \varepsilon_v^m}{\partial t}. \quad (41)$$

In the micropore, the full equation has to be implemented

$$n^m S_e^m \frac{\partial C^m}{\partial t} = \nabla(D_e \nabla C^m) - (1 - \omega) \nabla(v^m C^m) + Q_c^m - C^m \left(n^m \frac{\partial S_e^m}{\partial t} + S_e^m \frac{\partial \varepsilon_v}{\partial t} \right). \quad (42)$$

It is hypothesized here that the micropore is always nearly saturated. Therefore, the solute transport equation for the micropore can be reduced to

$$n^m \frac{\partial C^m}{\partial t} = \nabla(D_e \nabla C^m) - (1 - \omega) \nabla(v^m C^m) + Q_c^m - C^m \frac{\partial \varepsilon_v^m}{\partial t}. \quad (43)$$

Note that the membrane coefficient ω is calibrated here with data from Rowe and Brachman [42] and is found to be in the range 0.97–0.98. This gives an effective diffusion coefficient ratio (also given by Musso et al. [34]) in the range of 0.02–0.03,

$$D_e/D_0 = (1 - \omega) \quad (44)$$

According to Eq. (11), the apparent diffusion coefficient $D_a/D_0 = 0.05$ – 0.075 when $n = 0.41$ falls exactly on the regressed line in Fig. 4. Therefore, the calibrated membrane coefficient reasonably reflects the constricting effect of the diffuse layer at the clay–water interface. It also

suggests the viability of the above form of expression Eq. (44).

The mass exchange flux Q_c is given as a function of fluid exchange rate a^M (flow out of micropore as $a^M > 0$) and mass transfer coefficient \bar{D} ,

$$Q_c^M = (1 - \omega) \left[-a^M C^M + \bar{D}(C^m - C^M) \right] \quad (45)$$

And

$$Q_c^m + Q_c^M = 0. \quad (46)$$

The convective mass flux is directional with respect to which concentration (i.e. C^m or C^M) is carried by the fluid flow. We define

$$C^M = \begin{cases} C^m, & \text{if } a^M \geq 0 \\ C^M, & \text{if } a^M < 0 \end{cases} \quad (47)$$

The fluid exchange rate a^M is governed by pore pressure and osmotic suction differences. The mass transfer coefficient can be approximated to be

$$\bar{D} = \frac{D_e}{L_c} \quad (48)$$

where L_c is the characteristic length of the clay aggregate. Musso et al. [34] proposed a similar concept of mass exchange between dual porosities and developed a mathematical equation in exponential form for the transfer coefficient

$$\bar{D} = \alpha \exp(-HC^M) \quad (49)$$

where α and H are two parameters to be calibrated by experiments, which were reported to be 0.8 and 8, respectively, for MX-80 bentonite in contact with NaCl solution [34].

It is assumed in this study that the salinity in the micropore dominates the mass exchange rate. Inside the clay aggregate, the void ratio is greatly dependent on the DDL behaviour. We modify Eq. (49) to correlate the transfer coefficient with the chemical concentration in micropore

$$\bar{D} = \frac{D_e}{L_c} \exp(-HC^m). \quad (50)$$

Our numerical simulation of brine–bentonite interaction leads to the following set of parameters, i.e. $L_c = 10 \mu\text{m}$, $H = 0.004$ (B_{1.6} sample) for salinity C^m in the unit of molar/m³.

1.9 Constitutive relationship for mechanical behaviour

The general constitutive relationship for the mechanical behaviour of unsaturated expansive soil can be given as

$$\sigma = \mathbf{D} \cdot (\varepsilon - \varepsilon_p - \varepsilon_s) \quad (51)$$

where σ is the total stress, \mathbf{D} is the elastic stiffness matrix, ε_p is the plastic strain and ε_s is the swelling strain that occurs mainly from the expansion/shrinkage of the DDL in the micropore. In the case of constant volume swelling, the plastic strain is assumed to be negligible.

Assuming that the degree of saturation in the micropore is close to 1, the void ratio e_m is related to the water content w^m through the phase relationship $e_m = G_s w^m = (\rho_s/\rho_w) \cdot w^m$, where ρ_w is the density of pure water. The microporosity is then linearly correlated with the gravimetric water content (w) in the form of

$$w^m = \frac{e_m X \rho_l}{\rho_s} \quad (52)$$

where X is mass ratio of water over total mass of saline water and ρ_l is the density of saline water, which is larger than that of pure water. Therefore, the swelling strain associated with the micropore deformation is given as

$$d\varepsilon_s = \frac{\rho_s}{X \rho_l} \frac{dw^m}{1 + e_0} \quad (53)$$

where w^m is gravimetric water content in the micropore. In accord with model assumption (c), and supported by the analysis of WRC in the double structures, the micropore water content can be approximated as equal to the total gravimetric water content, i.e. $w^m \cong w_{\text{total}}$.

The mass ratio X is not a constant. A linear function of X for saline water of various concentrations leads to the following correlation

$$X = 1 - 5.87 \times 10^{-5} * C. \quad (54)$$

In this study, the mass of 1 L model water was measured as 1223.1 g. The total dissolved salt (TDS) of the Queen's University's model water (MW) supernatant was 328.9 g/L. In this case, the mass of DI water (894.2 g) was calculated as 73% of the mass of 1 L of MW2 supernatant. Therefore, $X = 0.73$ is justifiable for saline water of $\rho_l = 1223 \text{ kg/m}^3$. Then, $e_m = \frac{w \rho_s}{X \rho_l} = \frac{2.75}{0.73 * 1.223} w = 3.08 w$.

Using the above relationship, we can predict the ratio of micropore to total pore void ratios, defined as

$$f_m = \frac{e_m}{e_0}. \quad (55)$$

This parameter can be a viable measure to evaluate and validate the assumption of the micropore constitutive equation. Manca et al. [29] conducted MIP test to determine the macropore ($r > 1 \mu\text{m}$) void ratio for bentonite under permeation of 4 M saline at $e^M = 0.35$ for $e_0 = 0.78$, corresponding to the portion of microporosity $f_m = 0.55$. The osmotic suction of 4 M NaCl solution is reported as $\pi = 22.5 \text{ MPa}$ [26]. This leads to a calculated $w = 0.16$

from the WRC (Fig. 6). Then the micropore void ratio is given as $e_m = 2.9 * 0.16 = 0.464$, where the ratio 2.9 is the average of 2.75 and 3.08 for DI and brine solution, respectively. This corresponds to the portion of microporosity $f_m = 0.59$ and is close to the experimental results of $f_m = 0.55$ (7% variance error). Therefore, the proposed model is an acceptable approximate that can correlate the microporosity with water content.

Using this formula, we can analyse the double-porosity proportion by the water content and suction level for any bentonite samples. For instance, the initial condition of the as-compacted bentonite specimen (by Queen's University) is $w_0 = 0.11$, $\rho_d = 1.6 \text{ g/cm}^3$, which indicates $e_m = 0.3$ and $f_m = 0.42$. When saturated with brine, the osmotic suction level of 40 MPa corresponds to a gravimetric water content of 0.15. At a dry density of 1 g/cm^3 , this results in a micropore void ratio $e_m = 3.08 w$ and the portion of microporosity $f_m = 0.643$, which is much less than 1.0, suggesting a significant portion of macropore even at full saturation.

1.10 Finite element model for constant volume swelling test

The following governing equations of the model are implemented and solved in COMSOL (V 5.3).

$$\begin{aligned} \nabla \cdot \sigma &= 0 \\ n^m \frac{\partial C^m}{\partial t} &= \nabla D_e \nabla C^m - (1 - \omega) \nabla (v^m C^m) \\ &\quad + Q_c^m - C^m \frac{\partial \varepsilon_v}{\partial t} \\ n^M S_e^M \frac{\partial C^M}{\partial t} &= D_0 \nabla^2 C^M - \nabla (v^M C^M) \\ &\quad + Q_c^M - C^M n^M \frac{\partial S_e^M}{\partial t} \\ \frac{\partial}{\partial t} (\rho_l n^m) - \nabla \frac{k_s^m}{\mu} \rho_l (\nabla p^m - k_c \nabla C^m) &= Q_m \\ G_s \rho_l w^M \left(C_m \frac{\partial p^M}{\partial t} + C_s \frac{\partial C^M}{\partial t} \right) \\ &\quad - \nabla \frac{k_s^M k_r}{\mu} \rho_l (\nabla p^M - k_c \nabla C^M) = -G_s \rho_l w \frac{\partial \varepsilon_v^M}{\partial t} + Q_M \end{aligned} \quad (56)$$

where the storage terms are given as $C_m = (1 - n^M) \left(\chi_f + \frac{B}{\rho^M w^M} \right) - n^M \chi_s$ and $C_s = n^M \chi_s k_c + (1 - n^M) \frac{k_2}{\rho_l}$.

Table 1 shows the input parameters. Extensive simulation trials have been carried out to determine an appropriate range for these input parameters. The parameters shown are to the ones that best reproduce the experimental data.

Table 1 Model input parameters

Variable	Unit	Value/expression	
		Validation A (Posiva data)	Validation B (Queen's U data)
<i>Initial conditions</i>			
G_s		2.75	2.75
ρ_d		1.7	1.6
e_0		$G_s/1.7-1$	$G_s/1.6-1$
w_0		0.05	0.11
e_m		Equation (6)	Equation (6)
<i>Saturated permeability</i>			
k_s^M	m/s	$4*k^m$	Equations (7–8)
k_s^M	m/s	2*Equation (5)	Equation (5)
<i>Relative permeability</i>			
k_r^m		S_e^3	1
k_r^m		$(0.8)^6$	1
<i>Chemo-osmosis</i>			
ω		–	0.97–0.98
k_c	Pa m ³ /mol	–	8.83E3
Mass exchange			
$\bar{\alpha}$	m/Pa s	$2* k^m*\rho_l$	$10*k^m*\rho_l$
D_e	m ² /s	–	Equation (12)
L_c	m	–	1E–5
\bar{D}	m/s	–	Equation (50)
H	m ³ /mol	–	0.004–0.005
Q^M	m/s	–	Equation (45)
<i>Solute transport</i>			
D_0	m ² /s	–	1E–9
τ^m	–	–	$D_0/\text{Eq. (12)}$
τ^M	–	–	1
Water retention curve			
S_u^m	Pa	From Eq. (14)	From Eq. (14)
S_{ut}	Pa	2800	Equation (15)
S_u^M	Pa	From Eq. (13)	From Eq. (13)
<i>Mechanical property</i>			
K	MPa	36.4	19.3 (DI) 19.3 (MW)
Boundary condition			
\mathbb{L}	m/s	$0.5E7*k^M$	$0.5E7*k^M$
P_{in}	MPa	2	0.015
C_{in}	M	0	4.6
Dimension			
Radius	mm	25	19
Height	mm	65	12

C is chemical concentration in (mol/m³)

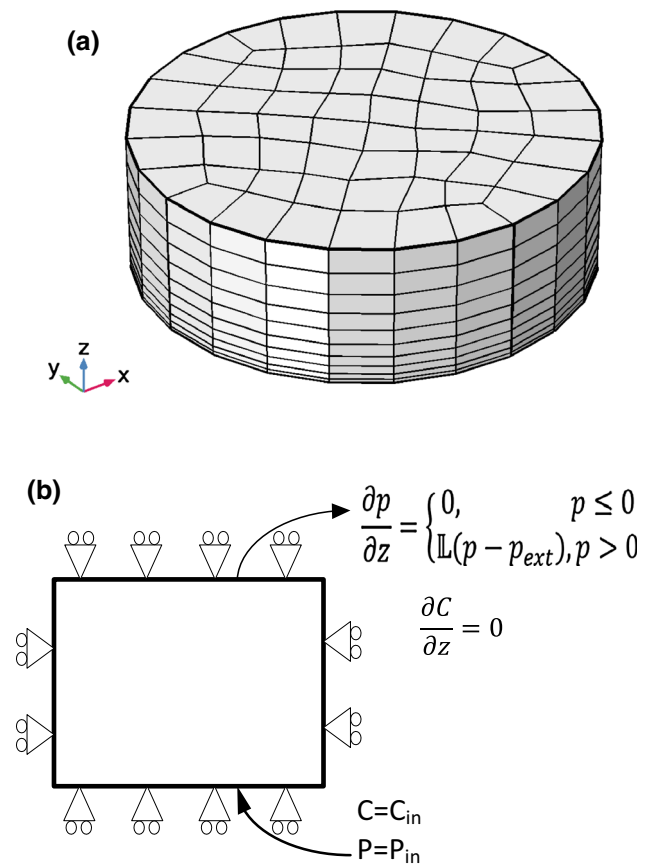
**Fig. 9** FEM model for the constant volume swelling test (a) and hydraulic–mechanical–chemical boundary conditions (b)

Figure 9 shows the finite element discretization and boundary conditions of the compacted bentonite specimen infiltrated with either DI water (Posiva test) or brine (Queen's University test). The bottom boundary is connected to the supply of permeant at constant pressure, while the top boundary is left open to ambient atmospheric pressure prior to flow through. Once pore fluid penetrates through the specimen, the top boundary is maintained as highly permeable and well drained to avoid water pressure build-up. This is a mixed Robin-type boundary condition given as

$$\frac{\partial p}{\partial z} = \begin{cases} 0, & p \leq 0 \\ L(p - p_{ext}), & p > 0 \end{cases} \quad (57)$$

where \mathbb{L} is a flow transfer coefficient shown in Table 1, p_{ext} is the target pressure (0 MPa in this work). The side wall is as assumed to be impermeable. The bottom boundary is kept at a constant chemical concentration equal to the one of the brine inflow. The top end is Neumann-type boundary for solute transport.

1.11 Simulation of Posiva test

This case addressed the experimental results of Posiva THM-coupled investigations, from a single series of test data (#100416) reported by Pintado et al. [40]. As a first step of validation of the HM coupling, the data on infiltration of low salinity water through MX-80 bentonite column were selected for analysis and modelling. A compacted MX-80 bentonite column with dry density at 1.7 g/cm^3 and initial water content of about 5% was infiltrated with low salinity water (salinity 0.87 g/L). The pressure head was maintained at 2 MPa for the inlet, while the outlet was open to ambient atmospheric pressure. The specimen has a diameter of 5 cm and a height of 6.3 cm. Figure 10 shows the sketch of the test and the instrumentation.

Due to the very low salinity of the permeant, the modelling ignored the effect of pore fluid chemistry and considered mainly the interaction between macropores and micropores. As shown in Table 1, most of the model parameters are the same as what we derived theoretically for MX-80 bentonite. These include the micropore void ratio and the water retention curves for both the micropore and macropore. Only minor adjustments were made with respect to the permeability and unsaturated state variables

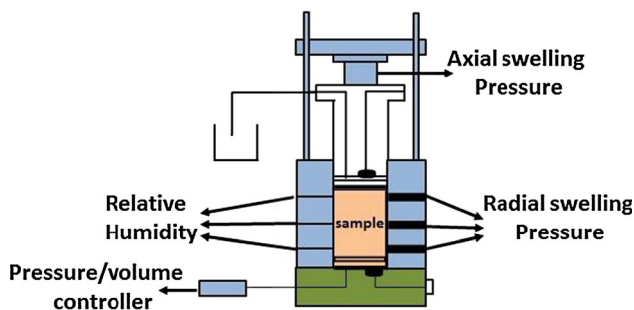


Fig. 10 Schematic diagram of the Posiva infiltration test set-up [40]

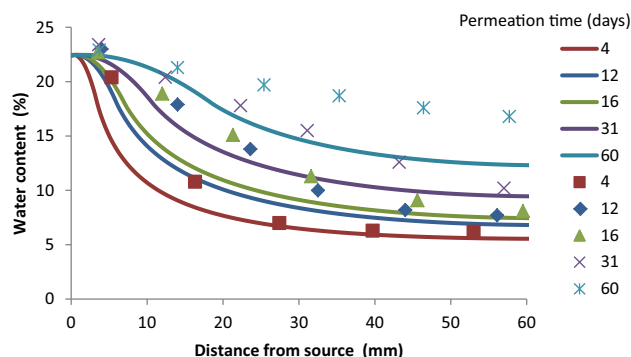


Fig. 11 Posiva test: distribution of water content at various permeation time (days)—the modelling results (solid lines) are compared with the experimental data (dots)

Figures 11, 12, 13 and 14 show the modelling results and the comparison with experimental data in terms of water content profile, suction profile, inflow volume and measured swelling pressure. It can be seen from those figures that the water infiltration volume and the suction profile are both well reproduced. The modelled swelling pressure compares well with the measured value, both in trend and magnitude. Although a discrepancy is found in the water content profile, the movement of the water front from the inlet towards the outlet is consistent with the experimental results. This is likely due to the variability in WRC, as the water content is computed on the basis of the water retention curve. It is shown that the total volume of water injection at the end of test after 2 months remains very small compared to the total volume of the soil specimen (32 mL vs. 124 mL), indicating a very low permeability in the specimen. Using a bulk modulus ($K = 36.4 \text{ MPa}$) in the model is found to result in a satisfying prediction of the swelling pressure. However, the oedometer measurement ($K = 43.5 \text{ MPa}$) is somewhat higher than the modelling input.

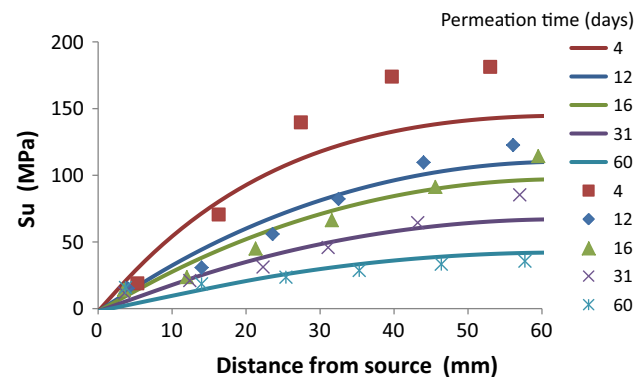


Fig. 12 Posiva test: distribution of matric suction at various permeation time (days)—the modelling results (solid lines) are compared with the experimental data (dots)

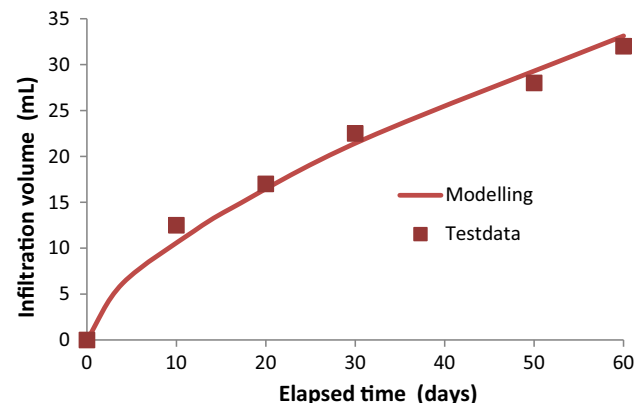


Fig. 13 Posiva test: variation of inflow volume with elapsed permeation period of time (days)

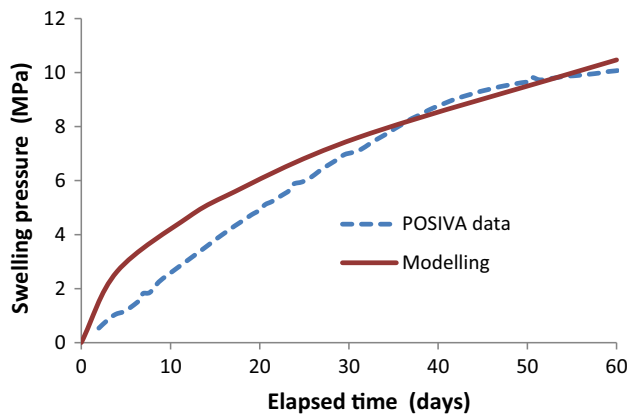


Fig. 14 Posiva test: the measured and modelled temporal variation of swelling pressure

1.12 Simulation of Queen's University tests

1.12.1 Experimental results of temporal variation of swelling pressure

The CNSC initiated a collaborative research with Queen's University to study the chemical influences on swelling behaviours of MX-80 bentonite under various dry densities with permeation of two types of pore fluid, i.e. DI water and MW (highly concentrated brine). The MW has a molarity of 4.6 M and is mainly composed of NaCl, KCl, CaCl_2 and MgSO_4 . Both bentonite and sand/bentonite mixture were investigated. The experimental results for the variation of swelling pressure under constant volume conditions are presented in Fig. 15. Table 2 provides a summary description of the tests with their acronyms.

Pore fluid chemistry has a significant impact on the swelling of bentonite as shown in Fig. 15. With the same dry density, DI water infiltration results in a peak swelling pressure about three times higher than the MW case. Within 500 h, no obvious variation in swelling pressure for the case of DI water can be noticed from the test data. After 500 h, the swelling pressure gradually decreases and reached a stable value by 2000 h for DI water, while for MW, the swelling pressure took much longer to stabilize after 8000 h of continuous permeation. The swelling pressure for DI water decreases by approximately 10% from the peak, whereas for MW, a decrease of 80–90% from the peak was observed. Sand–bentonite mixtures (SB) show a very similar swelling behaviour with bentonite with the same value in EMDD. Our modelling efforts will focus on reproducing the gradual decrease in swelling pressure under hydration of brine water.

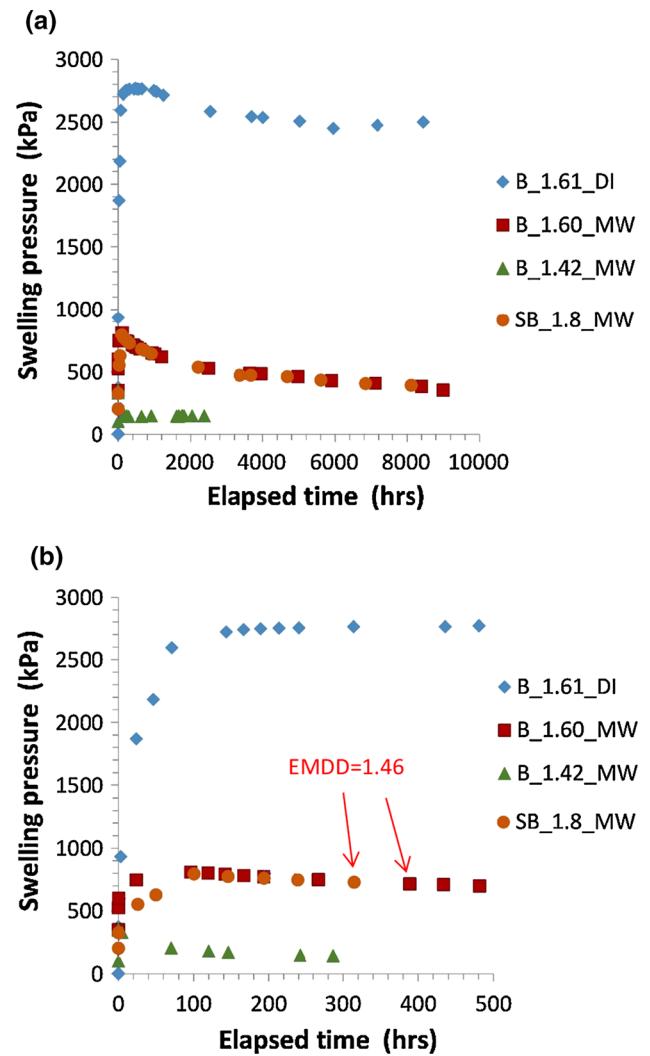


Fig. 15 Variation of swelling pressure with elapsed time for MX-80 at different dry densities and pore fluid scenarios **a** long-term behaviour and **b** short-term behaviour [42]

Table 2 Experimental conditions for Queen's University dataset

Sample ID	Soil composition	Dry density (g/cm ³)	Permeant
B_1.61_DI	Bentonite MX-80	1.61	DI water
B_1.60_MW	Bentonite MX-80	1.60	Model water (brine)
B_1.42_MW	Bentonite MX-80	1.42	Model water (brine)
SB_1.8_MW	Bentonite 70% Sand 30%	1.80	Model water (brine)

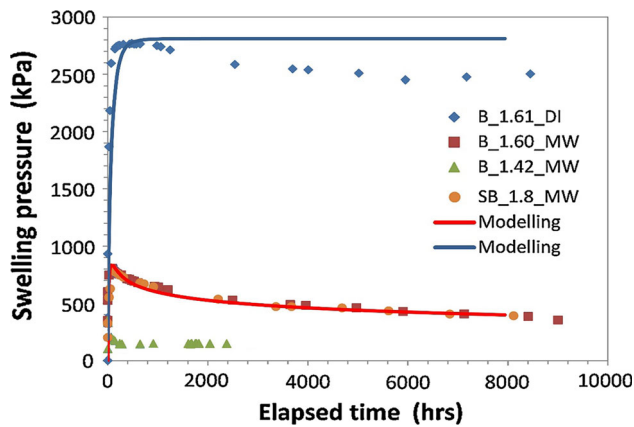


Fig. 16 Temporal variation of swelling pressure of MX-80 bentonite under permeation of DI water and brine

1.12.2 Modelled temporal variation of swelling pressure

Figure 16 compares the modelling and measured results for swelling pressure. It is shown that the model simulates very well the pressure transient. Consistent with the experimental data, the model was able to reproduce the substantial long-term decrease in swelling pressure in the MW case. The model also shows that a much higher swelling pressure was developed for the DI water case, at early time, and did not decrease in the long term. The experimental data show, however, a decay of swelling pressure even for the DI case, although it is less pronounced as in the MW case. It is believed that this is due to a redistribution of chemicals like sodium ions between the double-porosity structures. Sodium ions are originally present in MX-80 bentonite crystalline structures predominantly in the

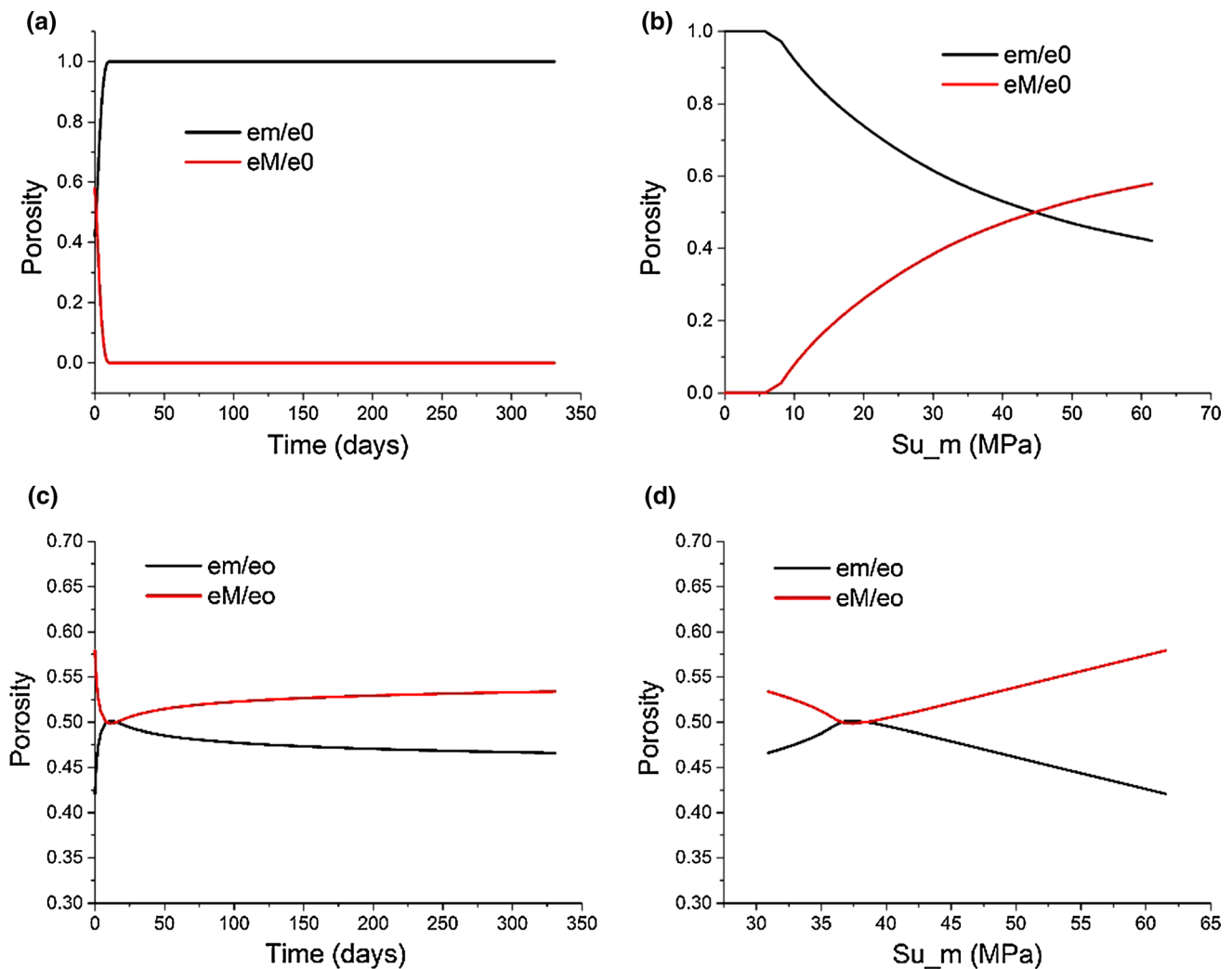


Fig. 17 Variation of pore fractions with time and matric suction for bentonite permeated with DI water (a, b) and brine solution (c, d)

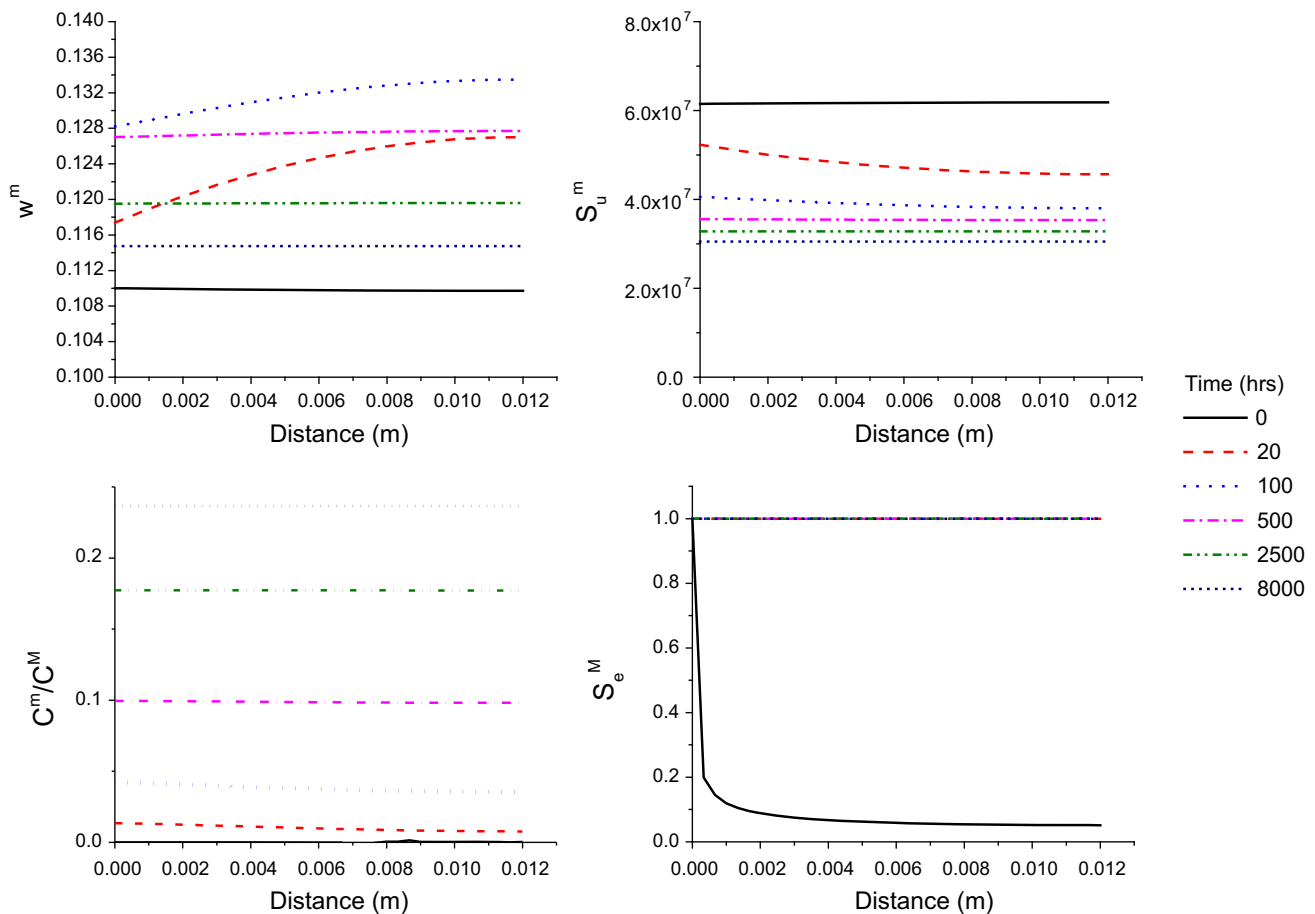


Fig. 18 Variation of parameters with change in distance from inlet for the permeation of brine solution

micropores, but later migrate into the macropore space and reducing the balance of osmotic suction between the two pore types. Using the current theoretical framework, this phenomenon can be further investigated in order to provide better understanding and quantification. This will be the subject of future investigations.

Figure 17a–d shows the modelled results for variation of microporosity and macroporosity with time and suction. The micropore fraction is found to increase generally with decrease in suction. The brine solution substantially suppresses the expansion of micropores, with a much smaller growth rate in wetting stage compared to DI water. The trend of micropore variation is consistent with the experimental observation of the swelling pressure.

Figure 18 shows the modelled profile of several variables at different permeation periods. The macropore reaches full saturation within a few days. In the meanwhile, micropore water content and matric suction is still changing. Mass exchange between the two pore structures leads to a gradual increase of micropore salinity, which remains lower than that of the macropore for the whole simulation period.

Figure 18 gives a brief illustration of the overall HMC-coupled processes occurring in MX-80 bentonite under permeation of brine. It is shown that the micropore water content w^m varies significantly with time at different locations. At 100 h, the modelled w^m reaches a peak value at regions close to the outlet boundary, where e^M remains in a low level before the chemical front passes that point. In the beginning, the macropore becomes saturated quickly, while chemical transport therein is delayed compared to the water movement due to chemical exchange with the micropore. In regions further away from the inlet, water would be preferentially absorbed into the micropore because of the lack of osmotic suction gradient. The swelling pressure peak may be correlated with the chemical front in the macropore. The extremely concentrated brine poses a very high osmotic suction on the clay aggregate that draws water from the micropore, causing a decrease of the microporosity and then a decline of the swelling pressure. This observation corresponds well to the conceptual model and seems well justified.

2 Conclusion

In this study, a HMC-coupled model was developed for compacted unsaturated bentonite. The model is based on a dual-porosity framework and considers the effect of salinity on various hydraulic and mechanical properties. A series of relationships for HMC properties have been proposed for MX-80 bentonite. Effective approaches to estimate the WRC and hydraulic conductivity for each porosity component were proposed and verified. The coupled HMC model was used to simulate laboratory swelling experiments on compacted MX-80 bentonite specimens infiltrated with DI water and brine, respectively. A good agreement between the model results and the experimental data, both in trends and absolute values, suggest that the main processes have been captured.

Many of the parameters representative of the hydraulic–chemical characteristics of the bentonite are derived by best-fit correlations of available data from the literature combined with the ones determined from laboratory tests at Queen’s University. Despite the variability of the data sources, these empirical correlations when used as input to the proposed model are able to reproduce the main processes found from swelling tests performed at two different laboratories. Further in-depth microporosimetric studies, as part of CNSC’s ongoing regulatory research, are being conducted at Queen’s University in order to verify, calibrate and further refine the current model and improve our understanding of the effects of salinity on the swelling potential of bentonite.

Open Access This article is distributed under the terms of the Creative Commons Attribution 4.0 International License (<http://creativecommons.org/licenses/by/4.0/>), which permits unrestricted use, distribution, and reproduction in any medium, provided you give appropriate credit to the original author(s) and the source, provide a link to the Creative Commons license, and indicate if changes were made.

References

- Agus SS, Arifin YF, Tripathy S, Schanz T (2013) Swelling pressure-suction relationship of heavily compacted bentonite-sand mixtures. *Acta Geotech* 8(2):155–165. <https://doi.org/10.1007/s11440-012-0189-0>
- Akesson M, Jacinto AC, Gatabin C, Sanchez M, Ledesma A (2009) Bentonite THM behaviour at high temperatures: experimental and numerical analysis. *Geotechnique* 59(4):307–318. <https://doi.org/10.1680/geot.2009.59.4.307>
- Alonso EE, Romero E, Hoffmann C (2011) Hydromechanical behaviour of compacted granular expansive mixtures: experimental and constitutive study. *Geotechnique* 61(4):329–344. <https://doi.org/10.1680/geot.2011.61.4.329>
- Bourg IC, Sposito G, Bourg ACM (2007) Modeling cation diffusion in compacted water-saturated Na-bentonite at low ionic strength. *Environ Sci Technol* 41(23):8118–8122
- Bradbury MH, Baeyens B (2011) Physico-Chemical Characterisation Data and Sorption Measurements of Cs, Ni, Eu, Th, U, Cl, I and Se on MX-80 Bentonite. *Nucl Energy Saf Res Dep Lab Waste Manag*. ISSN 1019-0643
- Carmen PC (1938) The determination of the specific surface of powders. *J Soc Chem Ind Trans* 57:225
- Carrier WD III (2003) Goodbye, Hazen; hello, Kozeny–Carman. *J Geotech Geoenviron Eng* 129(11):1054–1056. [https://doi.org/10.1061/\(ASCE\)1090-0241\(2003\)129:11\(1054\)](https://doi.org/10.1061/(ASCE)1090-0241(2003)129:11(1054))
- Della Vecchia G, Musso G (2016) Some remarks on single- and double-porosity modeling of coupled chemo-hydro-mechanical processes in clays. *Soils Found* 56(5):779–789. <https://doi.org/10.1016/j.sandf.2016.08.004>
- Dieudonne AC, Gatabin C, Talandier J, Collin F, Charlier R (2016) Water retention behaviour of compacted bentonites: experimental observations and constitutive model. In: Delage P, Cui YJ, Ghabezloo S, Pereira JM, Tang AM (eds) *E3S Web of conferences 3rd European conference on unsaturated soils—E-Unsat 2016*, vol 9. <https://doi.org/10.1051/e3sconf/20160911012>
- Dieudonne A-C, Della Vecchia G, Charlier R (2017) Water retention model for compacted bentonites. *Can Geotech J* 54(7):915–925. <https://doi.org/10.1139/cgj-2016-0297>
- Dixon DA, Man A, Stone J, Rimal S, Siemens G, Abootalebi P, Birch K (2016) Backfilling and sealing materials for a deep geological repository. In: 3rd Canadian conference on nuclear waste management, decommissioning and environmental restoration, Ottawa, ON, Canada
- Do Guimarães LN, Gens A, Sánchez M, Olivella S (2013) A chemo-mechanical constitutive model accounting for cation exchange in expansive clays. *Geotechnique* 63(3):221–234
- Fernandez AM, Villar MV (2010) Geochemical behaviour of a bentonite barrier in the laboratory after up to 8 years of heating and hydration. *Appl Geochem* 25(6):809–824. <https://doi.org/10.1016/j.apgeochem.2010.03.001>
- Fredlund DG, Rahardjo H, Fredlund MD (2012) *Unsaturated soil mechanics in engineering practice*. Wiley, Hoboken
- Gens A, Sanchez M, Guimaraes LDN, Alonso EE, Lloret A, Olivella S, Villar MV, Huertas F (2009) A full-scale in situ heating test for high-level nuclear waste disposal: observations, analysis and interpretation. *Geotechnique* 59(4):377–399. <https://doi.org/10.1680/geot.2009.59.4.377>
- Gens A, Guimaraes LDN, Sanchez M, Vallejan B (2011) Coupled analysis of double porosity swelling clays. In: Borja RI (ed) *Multiscale and multiphysics processes in geomechanics: results of the workshop on multiscale and multiphysics processes in geomechanics*. Springer, Berlin, pp 85–88
- Gens A, Vallejan B, Sanchez M, Imbert C, Villar MV, Van Geet M (2011) Hydromechanical behaviour of a heterogeneous compacted soil: experimental observations and modelling. *Geotechnique* 61(5):367–386. <https://doi.org/10.1680/geot.SIP11.P.015>
- Herbert HJ, Kasbohm J, Sprenger H, Fernández AM, Reichelt C (2008) Swelling pressures of MX-80 bentonite in solutions of different ionic strength. *Phys Chem Earth* 33(SUPPL. 1):S327–S342. <https://doi.org/10.1016/j.pce.2008.10.005>
- Hoffmann C, Alonso EE, Romero E (2007) Hydro-mechanical behaviour of bentonite pellet mixtures. *Phys Chem Earth* 32(8–14):832–849. <https://doi.org/10.1016/j.pce.2006.04.037>
- Jo HY, Katsumi T, Benson CH, Edil TB (2001) Hydraulic conductivity and swelling of nonprehydrated GCLs permeated with single-species salt solutions. *J Geotech Geoenviron Eng* 127:557–567
- Keijzer TJS, Klingeld PJ, Loch JPG (1999) Chemical osmosis in compacted clayey material and the prediction of water transport. *Eng Geol* 53(2):151–159. [https://doi.org/10.1016/S0013-7952\(99\)00028-9](https://doi.org/10.1016/S0013-7952(99)00028-9)

22. Kozeny J (1927) Ueber kapillare Leitung des Wassers im Boden. Wien, Akad Wiss 136(2a):271
23. Krahn J, Fredlund DG (1972) On total, matric and osmotic suction. *Soil Sci* 114(5):339–348
24. Li Z, Katsumi T, Inui T, Takai A (2013) Fabric effect on hydraulic conductivity of kaolin under different chemical and biochemical conditions. *Soils Found* 53(5):680–691. <https://doi.org/10.1016/j.sandf.2013.08.006>
25. Li Z, Xue Q, Katsumi T, Inui T (2014) Electric-hydraulic-chemical coupled modeling of solute transport through landfill clay liners. *Appl Clay Sci* 101:541–552
26. Luo Y, Roux B (2010) Simulation of osmotic pressure in concentrated aqueous salt solutions. *J Phys Chem Lett* 1(1):183–189. <https://doi.org/10.1021/jz900079w>
27. Malusis MA, Shackelford CD (2002) Chemico-osmotic efficiency of a geosynthetic clay liner. *J Geotech Geoenviron Eng* 128(2):97–106. [https://doi.org/10.1061/\(asce\)1090-0241\(2002\)128:2\(97\)](https://doi.org/10.1061/(asce)1090-0241(2002)128:2(97))
28. Man A, Martino JB (2009) Thermal, hydraulic and mechanical properties of sealing materials. NWMO, Toronto
29. Manca D, Ferrari A, Laloui L (2016) Fabric evolution and the related swelling behaviour of a sand/bentonite mixture upon hydro-chemo-mechanical loadings. *Geotechnique* 66:41–57. <https://doi.org/10.1680/jgeot.15.P.073>
30. Melkior T, Gaucher EC, Brouard C, Yahiaoui S, Thoby D, Clinard C, Ferrage E, Guyonnet D, Tournassat C, Coelho D (2009) Na⁺ and HTO diffusion in compacted bentonite: effect of surface chemistry and related texture. *J Hydrol* 370(1–4):9–20. <https://doi.org/10.1016/j.jhydrol.2009.02.035>
31. Murad MA, Moyne C (2008) A dual-porosity model for ionic solute transport in expansive clays. *Comput Geosci* 12(1):47–82. <https://doi.org/10.1007/s10596-007-9060-z>
32. Musso G, Romero Morales E, Gens A, Castellanos E (2003) The role of structure in the chemically induced deformations of FEBEX bentonite. *Appl Clay Sci* 23(1–4):229–237. [https://doi.org/10.1016/S0169-1317\(03\)00107-8](https://doi.org/10.1016/S0169-1317(03)00107-8)
33. Musso G, Della Vecchia G, Romero E (2013) Modeling the coupled chemo-hydro-mechanical behavior of compacted active clays. In: Manassero M, Dominijanni A, Foti S, Musso G (eds) *Coupled phenomena in environmental geotechnics*, 1st edn. CRC Press. ISBN 9781138000605
34. Musso G, Romero E, della Vecchia G (2013) Double-structure effects on the chemo-hydro-mechanical behaviour of a compacted active clay. *Geotechnique* 63(3):206–220
35. Nakashima Y (2006) H₂O self-diffusion coefficient of water-rich MX-80 bentonite gels. *Clay Miner* 41:659–668
36. Nasir O, Nguyen TS, Barnichon JD, Millard A (2017) Simulation of hydromechanical behaviour of bentonite seals for containment of radioactive wastes. *Can Geotech J* 54(8):1055–1070
37. Navarro V, Alonso EE (2000) Modeling swelling soils for disposal barriers. *Comput Geotech* 27(1):19–43. [https://doi.org/10.1016/S0266-352X\(00\)00002-1](https://doi.org/10.1016/S0266-352X(00)00002-1)
38. Navarro V, Asensio L, Yustres A, Pintado X, Alonso J (2013) Volumetric deformability and water mass exchange of bentonite aggregates. *Eng Geol* 166:152–159. <https://doi.org/10.1016/j.enggeo.2013.09.011>
39. Navarro V, Asensio L, De la Morena G, Pintado X, Yustres A (2015) Differentiated intra- and inter-aggregate water content models of mx-80 bentonite. *Appl Clay Sci* 118:325–336
40. Pintado X, Mamunul HM, Martikainen J (2013) Thermo-hydro-mechanical tests of buffer materials. In: POSIVA 2012-49. POSIVA, Eurajoki
41. Revil A (2017) Transport of water and ions in partially water-saturated porous media. Part 2. Filtration effects. *Adv Water Resour* 103:139–152. <https://doi.org/10.1016/j.advwatres.2016.07.016>
42. Rowe RK, Brachman RWI (2018) Laboratory determination of sealing material performance. Fifth progress report for R613.4. Queen's University, CNSC
43. Rueedi J, Marschall P (2011) Demonstration of gas-permeable seals for radioactive waste repositories—laboratory and in situ experiments. In: *Proceedings of the international conference on radioactive waste management and environmental remediation, ICEM*. pp 1413–1420. <https://doi.org/10.1115/icem2011-59224>
44. Salas J, Sena C, Arcos D (2014) Hydrogeochemical evolution of the bentonite buffer in a KBS-3 repository for radioactive waste. Reactive transport modelling of the LOT A2 experiment. *Appl Clay Sci* 101:521–532. <https://doi.org/10.1016/j.clay.2014.09.016>
45. Sanchez M, Gens A, Guimaraes LD, Olivella S (2005) A double structure generalized plasticity model for expansive materials. *Int J Numer Anal Meth Geomech* 29(8):751–787. <https://doi.org/10.1002/nag.434>
46. Sanchez M, Gens A, Olivella S (2012) THM analysis of a large-scale heating test incorporating material fabric changes. *Int J Numer Anal Meth Geomech* 36(4):391–421. <https://doi.org/10.1002/nag.1011>
47. Sanchez M, Gens A, Villar MV, Olivella S (2016) Fully coupled thermo-hydro-mechanical double-porosity formulation for unsaturated soils. *Int J Geomech*. [https://doi.org/10.1061/\(asce\)gm.1943-5622.0000728](https://doi.org/10.1061/(asce)gm.1943-5622.0000728)
48. Seiphoori A, Ferrari A, Laloui L (2014) Water retention behaviour and microstructural evolution of MX-80 bentonite during wetting and drying cycles. *Geotechnique* 64(9):721–734. <https://doi.org/10.1680/jgeot.14.P.017>
49. Shokri N, Zhou P, Keshmiri A (2015) Patterns of desiccation cracks in saline bentonite layers. *Transp Porous Media* 110(2):333–344. <https://doi.org/10.1007/s11242-015-0521-x>
50. Stewart DI, Studds PG, Cousens TW (2003) The factors controlling the engineering properties of bentonite-enhanced sand. *Appl Clay Sci* 23(1–4):97–110. [https://doi.org/10.1016/S0169-1317\(03\)00092-9](https://doi.org/10.1016/S0169-1317(03)00092-9)
51. Tachi Y, Yotsuji K (2014) Diffusion and sorption of Cs⁺, Na⁺, I[−] and HTO in compacted sodium montmorillonite as a function of porewater salinity: integrated sorption and diffusion model. *Geochim Cosmochim Acta* 132:75–93. <https://doi.org/10.1016/j.gca.2014.02.004>
52. Thyagaraj T, Salini U (2015) Effect of pore fluid osmotic suction on matric and total suctions of compacted clay. *Géotechnique* 65(11):952–960
53. Villar MV, Sanchez M, Gens A (2008) Behaviour of a bentonite barrier in the laboratory: experimental results up to 8 years and numerical simulation. *Phys Chem Earth* 33:S476–S485. <https://doi.org/10.1016/j.pce.2008.10.055>
54. Wersin P, Kiczka M, Koskinen K (2016) Porewater chemistry in compacted bentonite: application to the engineered buffer barrier at the Olkiluoto site. *Appl Geochem* 74:165–175. <https://doi.org/10.1016/j.apgeochem.2016.09.010>
55. Xie M, Agus SS, Schanz T, Kolditz O (2004) An upscaling method and a numerical analysis of swelling/shrinking processes in a compacted bentonite/sand mixture. *Int J Numer Anal Meth Geomech* 28(15):1479–1502. <https://doi.org/10.1002/nag.396>

Publisher's Note Springer Nature remains neutral with regard to jurisdictional claims in published maps and institutional affiliations.